Acta Oceanol. Sin., 2015, Vol. 34, No. 5, P. 110–116
DOI: 10.1007/s13131-015-0612-0
http://www.hyxb.org.cn
E-mail: hyxbe@263.net

Regional characteristics of sea ice thickness in Canadian shelf and Arctic Archipelago measured by Ground Penetrating Radar

LI Tao[1], ZHAO Jinping[1, 2*], JIAO Yutian[1], HOU Jiaqiang[1], MU Longjiang[1]

[1] Ocean University of China, Qingdao 266100, China

[2] Physical Oceanography Laboratory, Ocean University of China, Qingdao 266100, China

Received 6 July 2014; accepted 21 January 2015

Abstract

Ground Penetrating Radar (GPR) measurements of sea ice thickness including undeformed ice and ridged ice were carried out in the central north Canadian Archipelago in spring 2010. Results have shown a significant spatial heterogeneity of sea ice thickness across the shelf. The undeformed multi-year fast ice of (2.05±0.09) m thick was investigated southern inshore zone of Borden island located at middle of the observational section, which was the observed maximum thickness in the field work. The less thick sea ice was sampled across a flaw lead with the thicknesses of (1.05±0.11) m for the pack ice and (1.24±0.13) m for the fast ice. At the northernmost spot of the section, the undeformed multi-year pack ice was (1.54±0.22) m thick with a ridged ice of 2.5 to 3 m, comparing to the multi-year fast ice with the thickness of (1.67±0.16) m at the southernmost station in the Prince Gustaf Adolf Sea.

Key words: Arctic, sea ice thickness, Canadian Archipelago, Ground Penetrating Radar

Citation: Li Tao, Zhao Jinping, Jiao Yutian, Hou Jiaqiang, Mu Longjiang. 2015. Regional characteristics of sea ice thickness in Canadian shelf and Arctic Archipelago measured by Ground Penetrating Radar. Acta Oceanologica Sinica, 34(5): 110–116, doi: 10.1007/s13131-015-0612-0

1 Introduction

The thickness of sea ice has long been considered as a key indicator of climate change in the polar regions (Holt et al., 2009). Over the past few decades, however, the Arctic is undergoing significant changes in sea ice thickness and extent (Comiso, 2006; Deser and Teng, 2008; Haas et al., 2008; Kwok et al., 2009; Kwok and Rothrock, 2009; Tivy et al., 2011; Wadhams et al., 2011; Stroeve et al., 2012; Hansen et al., 2013; Bi et al., 2014), especially with a rapid reduction in the mean thickness of perennial Arctic sea ice during the 1990s as compared with earlier decades based on submarine-mounted upward looking sonar measurements of ice draft (Rothrock et al., 1999). The study of Arctic sea ice thickness is also aimed at understanding sea ice processes which occur on scales of metres to hundreds of metres, where processes are concerned not with the microstructure of an ice sheet but rather with physical, geochemical and biological couplings associated with sea ice features such as pressure ridges, meltwater pools and leads (Li et al., 2005; Wadhams et al., 2006).

To date, the useful observational methods of sea ice thickness mainly comprise: electromagnetic sounding from helicopter, laser freeboard swath sounding from aircraft, laser freeboard from satellite, radar altimetry from satellite, satellite-tracked buoys, moored and submarine-based upward looking sonar and drilling. Drill-hole is most accurate of all, but slow and tedious. EM industry can give a thickness distribution, but could be affected by porosity of ridges. Laser freeboard sounding from aircraft and satellite gives a wide distribution of freeboard of ice plus snow, which is difficult to convert to ice thickness unless we know the snow depth and density and ice density. Radar altimetry from satellite gives a global coverage up to latitude limit of satellite orbit but need a serious calibration-validation effort. Submarine-based sonar data are very expensive to sample and mooring-based sonar instruments do not have spatial data and are sometimes lost (Wadhams et al., 2006).

Ground penetrating radar (GPR), however, has often been used in previous studies in cold environments to investigate the properties of permafrost (Pilon et al., 1992) and glaciers, specially to measure changes in glacial mass balance both spatially and temporally (Winther et al., 1998; Pälli et al., 2002; Harper and Bradford, 2003; Sinisalo et al., 2003). Advantages of the GPR application in the Polar Regions are better portability and accuracy, which is very important in rigorous fieldworks. To measure the sea ice thickness using GPR, the relationship among physical structure, electromagnetic properties of sea ice and GPR's antenna frequency had been investigated with *in-situ* experiments and model analyses for years (Kovacs and Morey, 1978; Kovacs and Morey, 1979; Kovacs et al., 1987). Over the last decade, more portable GPR has been used to collect the data of sea ice thickness in the Polar Regions.

The Canadian Arctic Archipelago is an area covered mostly by thick multi-year ice which has critically been shrinking over past few decades, affecting the local surface heat balance and climate (Agnew et al., 2008; Howell et al., 2009; Kwok and Cunningham, 2010; Comiso, 2012; Howell et al., 2013). Sea ice thickness here as an important climate factor, however, has been known less due to the severe environment. Melling (2002) had examined the distribution of sea ice thickness over the Sverdrup Basin and discussed the driving factors based on the 123 703 samples from the

Foundation item: The National Natural Science Foundation of China under contract No. 41206174; China Postdoctoral Science Foundation under contract No. 2012M511546; the Key Project of Chinese National Science Fundation under contract No. 41330960.
*Corresponding author, E-mail: jpzhao@ouc.edu.cn

Panarctic Oils in 1970s. With those data, Johnston et al. (2009) found that the sea ice thickness in the Basin were (6.2±2.9) m. In Prince Gustaf Adolf Sea, the freeboard of 12 pieces of ridged ice ranged from 2.3 to 6.4 m, while the draft in half of them were reached to 25 m (Dickins and Wetzel, 1981). Submarine-based upper sonar data shown that mean ice draft was 4.5 m in M'Clure Strait (Mclaren et al., 1984) and 4–7 m northwestern Elizabeth Islands (Bourke and Garrett, 1987).

Although the sea ice thickness survey in the Canadian Arctic Archipelago has been started since 1980s, research on ice thickness with GPR has never been carried out in the central north Canadian Arctic Archipelago. In this paper, we introduce the principle of GPR measurement and data post-processing in Section 2. Then, the thickness distribution of the undeformed ice and ridged ice are discussed in Section 3. Finally, we conclude the field observations with GPR and give some suggestions on GPR measurements of sea ice thickness in future.

2 Methods

In spring 2010, the GPR measurements of sea ice thickness were carried out in the Canadian Arctic shelf with 5 stations (Fig. 1), including first-year ice, multi-year ice, pack ice and fast ice (Fig. 1). The instrument deployed in the fieldwork was a state of the art GPR, PulseEKKO PRO manufactured by Sensor & Software Inc. in Canada. Central frequency of the GPR antenna is 250 MHz. The instrumention of the GPR measurements could be seen in Fig. 2, which was comprised of the impulse velocity calibration (Fig. 2a) and towed operation (Fig. 2b), as with the GPR parameters setup shown in Table 1.

2.1 *Principles of GPR measurements of sea ice thickness*

GPR is radar that could transmit and receive the electromagnetic wave through antennae. Radar impulse is reflected when it hits a boundary with different dielectric constants. Because of the large difference in dielectric constants between sea water and ice, the receiving antenna of GPR on the ice surface records the two way travel time (T_{TWT}) of the impulse excited by transmitting antenna of the GPR. Thus, the thickness of sea ice (H) could accurately be estimated as the penetrating velocity of the wave (V_p) in sea ice known by

$$V_p T_{\mathrm{TWT}} = \left(x^2 + 4H^2\right)^{1/2} , \tag{1}$$

where x is the GPR's antenna separation. To get the T_{TWT} as accurate as possible from scan images, the reflection coefficient (R) and phrase of radar wave at the interface of ice and water should comprehensively be understood. In the GPR applications, the reflection coefficient R of the impulse was simplified as (Conyers, 2004; Trachtenberg, 2008):

$$R = \frac{\sqrt{\varepsilon_{\mathrm{r1}}} - \sqrt{\varepsilon_{\mathrm{r2}}}}{\sqrt{\varepsilon_{\mathrm{r1}}} + \sqrt{\varepsilon_{\mathrm{r1}}}} , \tag{2}$$

where the $\varepsilon_{\mathrm{r1}}$ and $\varepsilon_{\mathrm{r2}}$ are the dielectric constants of sea ice and water respectively. The reflection coefficient of a normal incident signal meeting the interface between an average dielectric value of sea ice ($\varepsilon_{\mathrm{r1}}$ = 3.7) and sea water ($\varepsilon_{\mathrm{r2}}$ = 81) (Winebrenner, 1989), will have R≈–0.65, which shows a heavily reflectance on the interface with a opposite wave phrase to that of the incident radar (Fig. 3a). Based on the reflection theory of electromagnetic wave, the interface can be determined at the zero in amplitude of the return pulse that is penetrating from the negative to positive phrase. Thereby, the T_{TWT} will accurately be chosen from the scans images to calculate the traveling distance of the impulse in sea ice given a penetrating velocity.

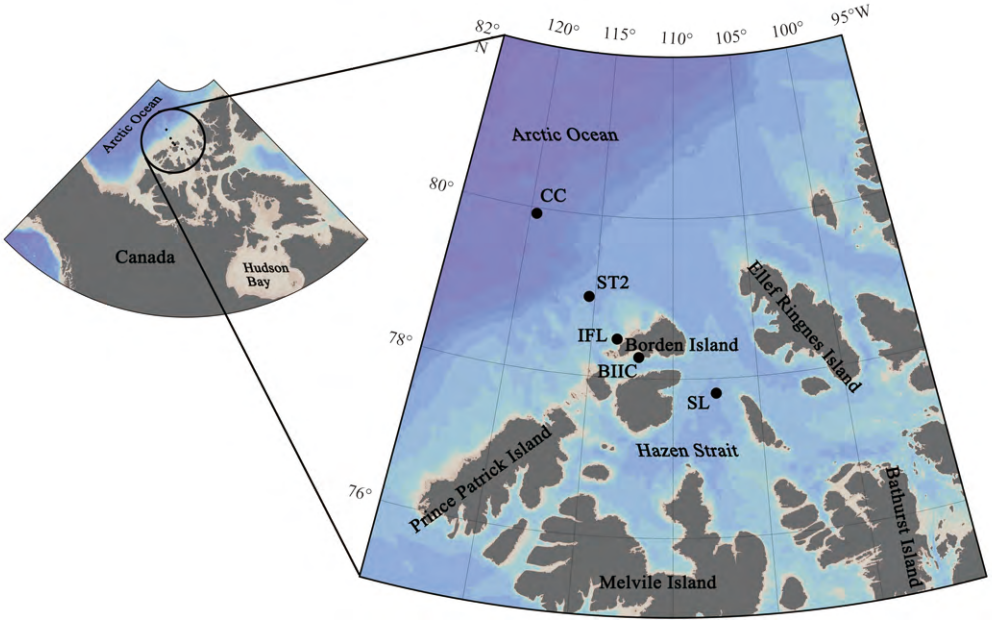

Fig. 1. Study area (black circle) and location of stations (black dots).

The travel velocity of an incident signal in sea ice could be computed with the *in-situ* velocity calibration (Fig. 2a). At each station, the top priority was to calibrate the wave propagation velocity due to its difference in sea ice of various ages. Based on the Eq. (1), the *in-situ* radar velocity in sea ice could be calculated with the two way travel time near the drilling hole and its practical thickness. Then, the GPR was towed on the target sea ice to collect the data of ice thickness.

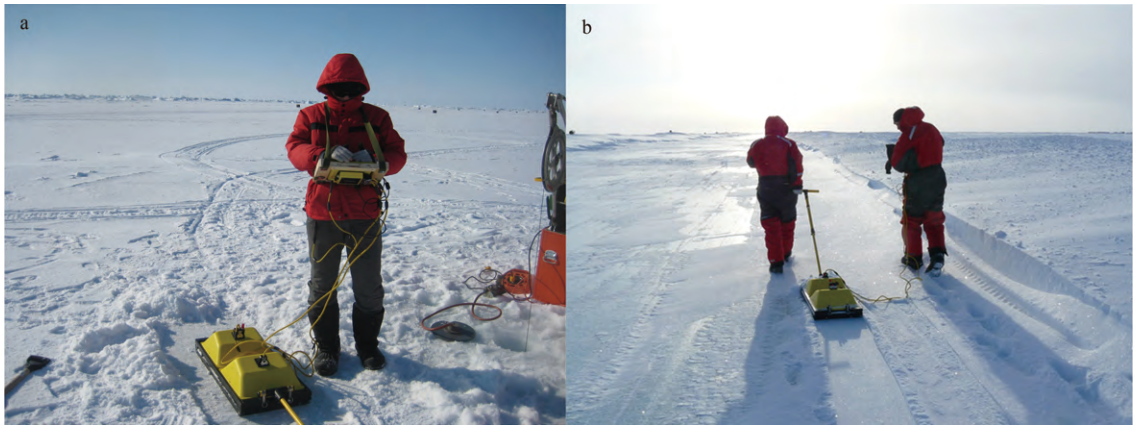

Fig. 2. *In-situ* operation of GPR measuring the ice thickness. a. Penetrating velocity calibration in the field and b. ice thickness measurement at station of BIIC south-western Borden Island.

Table 1. Set-up parameters of the pulse EKKO PRO in field

Parameters	Value
Antenna center frequency/wavelength	250 MHz/1.2 m
Antenna separation	0.38 m
Antenna type	linearly polarized half wavelength dipole
Time window/ns	72/100
System stacking	4
Survey mode	reflection

2.2 *Velocity calibration of GPR impulse in sea ice at station BIIC*

On 30th April 2010, the GPR measurements were taken place without the *in-situ* velocity calibration of radar in sea ice at the station BIIC. Fortunately, eight drilling ice thickness data on 26th April at the GPR section were collected (Table 2). According to the classical sea ice growth model, Stefan's Law (Stefan, 1891), the sea ice thickness at same spots on 30th were computed and corresponding mean penetrating velocity of radar in the sea ice was further calibrated with two way travel time of the GPR at the eight spots on 30th.

The Stefan's Law is based on the simple idea that the heat released by freezing at the ice bottom is conducted away through the ice by a constant temperature gradient. More precisely, Stefan's Law is based on the assumptions:

(1) no thermal inertia,

(2) no internal heat source,

(3) a known temperature at the top, T_0=$T_0(t)$,

(4) no heat flux from the water.

The analytic solution, with the initial condition H=H_0 for t=0, is

$$H^2 = H_0^2 + a^2 S, \tag{3a}$$

$$a^2 = 2k_i/\rho_i L, \tag{3b}$$

$$T_{\mathrm{at}} = \int_0^t [T_f - T_0(\tau)]\,\mathrm{d}\tau, \tag{3c}$$

where k_i is the heat conductivity of sea ice, ρ_i is the density of sea ice, L is the freezing latent heat, T_{at} is the negative accumulated temperature which is a sum of temperature difference between that at ice surface and local freezing point. The temperature at ice surface is usually instead of the surface air temperature T_0, while the T_{f} is the freezing point temperature of sea water.

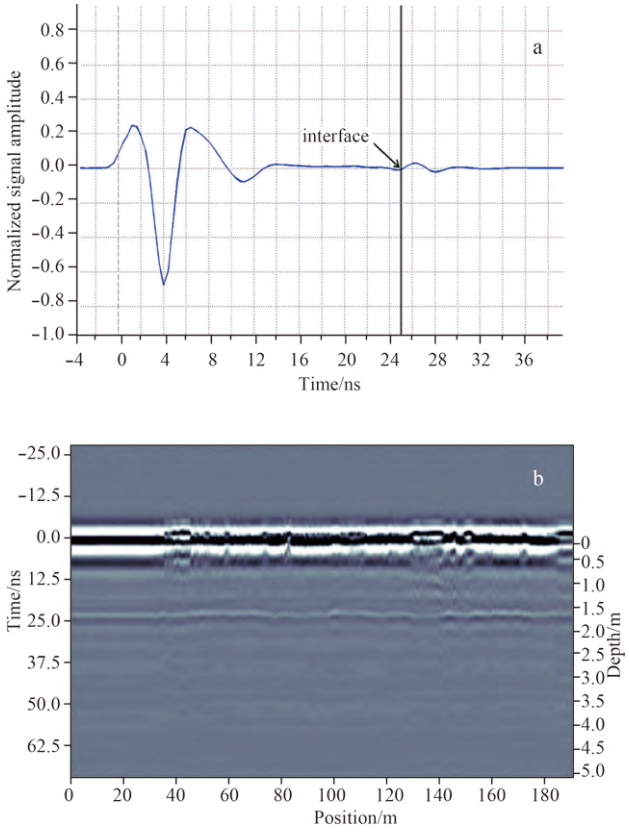

Fig. 3. Standard trace plot return (a) and pulse section (b) collected on 30 April at Sta. SL. The interface was determined at the zero in amplitude of the return pulse which is penetrating from the negative to positive phrase (a). At the section of 180 m, two ways return time was around 25 ns corresponding to the ice thickness was approximately 1.6 m with the electromagnetic wave velocity of 0.139 m/ns (b).

In our case, the surface air temperature T_0 at the station BIIC was from the NCEP–NCAR reanalysis dataset, while the freezing point temperature T_{f} was calculated by Millero formula (Millero and Leung, 1976):

$$T_{\mathrm{f}} = a_0 S + a_1 S^{1.5} + a_2 S^2 + bp, \tag{4}$$

where a_0= –0.057 5, a_1= 0.001 710 523, a_2= –0.000 215 499 6, b= –0.000 753, S and p are the salinity and pressure of sea water volume from the CTD measurements sampled 200 m away from the GPR section. Finally, the mean penetrating velocity of radar impulse in the sea ice at BIIC was 0.233 m/ns with an ice thickness growth of 1.3 cm in 4 d (Table 2).

Table 2. Velocity calibration of pulse through sea ice at the Sta. BIIC based on the drill-hole ice thickness data of four days ago

North latitude	West longitude	H_{di_26} [1)]/m	H'_{di_30} [2)]/m	T_{TWT}/ns	V_p'/m·ns^{-1}
78°16.13'	112°3.83'	2.210	2.219	18.0	0.248
78°16.13'	112°4.15'	2.070	2.080	17.5	0.239
78°16.13'	112°4.50'	1.940	1.951	17.5	0.224
78°16.13'	112°4.82'	2.050	2.060	18.2	0.227
78°16.15'	112°5.15'	2.100	2.110	18.0	0.235
78°16.15'	112°5.48'	2.030	2.040	17.5	0.234
78°16.17'	112°5.77'	2.000	2.010	18.2	0.222
78°16.17'	112°6.20'	1.940	1.951	16.8	0.233
Averaged		2.040	2.053	17.7	0.233

Notes: [1)] H_{dl_26}: drill–hole ice thickness on April 26th and [2)] H'_{di_30}: derived ice thickness on April 30th from the Stafen's Law and H_{dl_26}.

3 Results and discussion

In the Canadian Arctic shelf, the distribution feature of sea ice thickness has been examined at five stations where are across a flaw lead. In addition, a GPR section of ridged ice was collected with a clear ice-water interface, developing the *in-situ* GPR application on the sea ice thickness observation.

3.1 *Undeformed sea ice*

The undeformed ice thickness at stations CC, ST2 and IFL north of the Borden Island had various characteristics due to the dynamical process such as ice moving. At northernmost station CC, the main ice thickness was distributed between 1.5–1.7 m, while the ice of around 1.1 and 2 m was less investigated (Fig. 4a). The mean thickness at CC was (1.54±0.22) m, while the median, maximum and minimum of ice thickness were 1.59, 1.93 and 1.09 m respectively (Fig. 4f and Table 3). The mode of the ice thickness distribution H_{pm} (ice thickness at maximum probability density) at Sta. CC was 1.58 m (Fig. 4f). Nevertheless, the sea ice at Sta. ST2 north of a flaw lead was first–year pack ice, comparing to the first-year fast ice at Sta. IFL south of the flaw lead. The main ice thickness at those two stations covered between 1.1–1.3 m. Comparing the symmetrical probability density of sea ice at ST2, ice of 1.0–1.1 m thick at IFL was also well-monitored (Figs 4b and c). The mean thicknesses of them were (1.05±0.11) m for the pack floe and (1.24±0.13) m for the fast ice with the medians of 1.04 and 1.29 m. The maximum and minimum thicknesses of the first-year pack ice at Sta. ST2 were 1.14 and 0.88 m with a H_{pm} of 1.03 m, while those of the fast ice at IFL were 1.29 and 1.35 m with a H_{pm} of 1.31 m respectively (Fig. 4f and Table 3).

In the Canadian Arctic Archipelago, the GPR measurements were also carried out at Stas BIIC and SL where were covered by multi-year sea ice. The regional characteristics of sea ice thickness at these two stations are similar to those at ST2 and IFL with different magnitude: symmetric distribution at one of them (BIIC) and two peaks at another (SL). The main ice thickness at BIIC was about 1.9–2.1 m, while those at SL was about 1.2–1.3 and 1.7–1.8 m (Figs 4d and e). The mean sea ice thickness at BIIC was (2.05±0.09) m with the H_{pm} of 2.03 m that was the maximum value among five stations in this study, as the median, maximum and minimum of ice thicknesses were 2.05, 2.22 and 1.95 m respectively (Fig. 4b and Table 3). Similarly, the mean ice thickness at southernmost Sta. SL was (1.67±0.16) m with a H_{pm} of 1.76 m and a median of 1.74 m, which was significantly thinner than that in 3–5 m thick observed in Prince Gustaf Adolf Sea in winter 1970 (Melling, 2002).

Moreover, the mean sea ice thickness along with the entire section with 5 stations in Canadian Arctic shelf was obviously less than that at nine sections over the American Arctic investigated by Haas et al. (Haas et al., 2010) with the helicopter–based electromagnetic (EM) induction in spring 2009. One of the reasons was that Haas' sea ice thickness includes ridged ice information not just undeformed ice.

3.2 *Ridged ice*

Ridged ice constitute up to half of the volume of the ice in the Arctic. They are important biologically since they provide three-dimensional structure one scale up from the brine channel system, offering a substrate for algal growth and a feeding area and protected habitat for larger species. Large-scale ridged ice thickness observation has always been a scientific challenge because of the deforming and air or water trapped, even using the EM induction which is widely applied recently (Haas et al., 2010). A study of individual ridged ice, using first-year and multi-year ridges, would be very valuable, focusing on the structure and morphology of the ridges rather than their strength or the stresses involved in their formation (Wadhams et al., 2006). The Canadian Arctic Archipelago has long been covered by deformed sea ice that has significantly been thinned over the past decades. The thickness observations of ridged ice, as major kind of deformed ice, have attracted researcher's attention for years.

In our study, a GPR section of 300 m in the ridged ice was sampled at Sta. CC with a clear interface of ice and water (Fig. 5a). With the calibrated radar velocity in sea ice 50 m away from the GPR section, the probability density (Fig. 5b) and accumulative probability density (Fig. 5c) distributions of ridged ice thickness were obtained. The median of ridged ice thickness was 2.4 m with two peaks in Fig. 5b. The ice thickness at the first peak was about 1.5 m which presented the ridged ice's edge, while the thickness at the second peak was 2.8 m that shown the typical feature of the ridged ice here. Moreover, the ice thicknesses of 80% in the area were thinner than 3.0 m (Fig. 5c). Generally, the Canadian Arctic Archipelago is covered by the thickest sea ice around the Arctic Ocean, which mainly consists of the ridged pack ice and landfast ice. The pack ice ridge of 2.8 m at the Sta. CC is even thinner than the average ice thickness of 3.0 m in the Sverdrup Basin from March to May in 1979 (Melling, 2002).

The GPR image of ridged ice had clearly exhibited the thickness characteristics of deforming pack ice, revealing the per-

spective of GPR technique on the ridged ice thickness. Especially, the GPR observing technique for complicated deformed ice thickness in grid-scale requires more attention and efforts in the future.

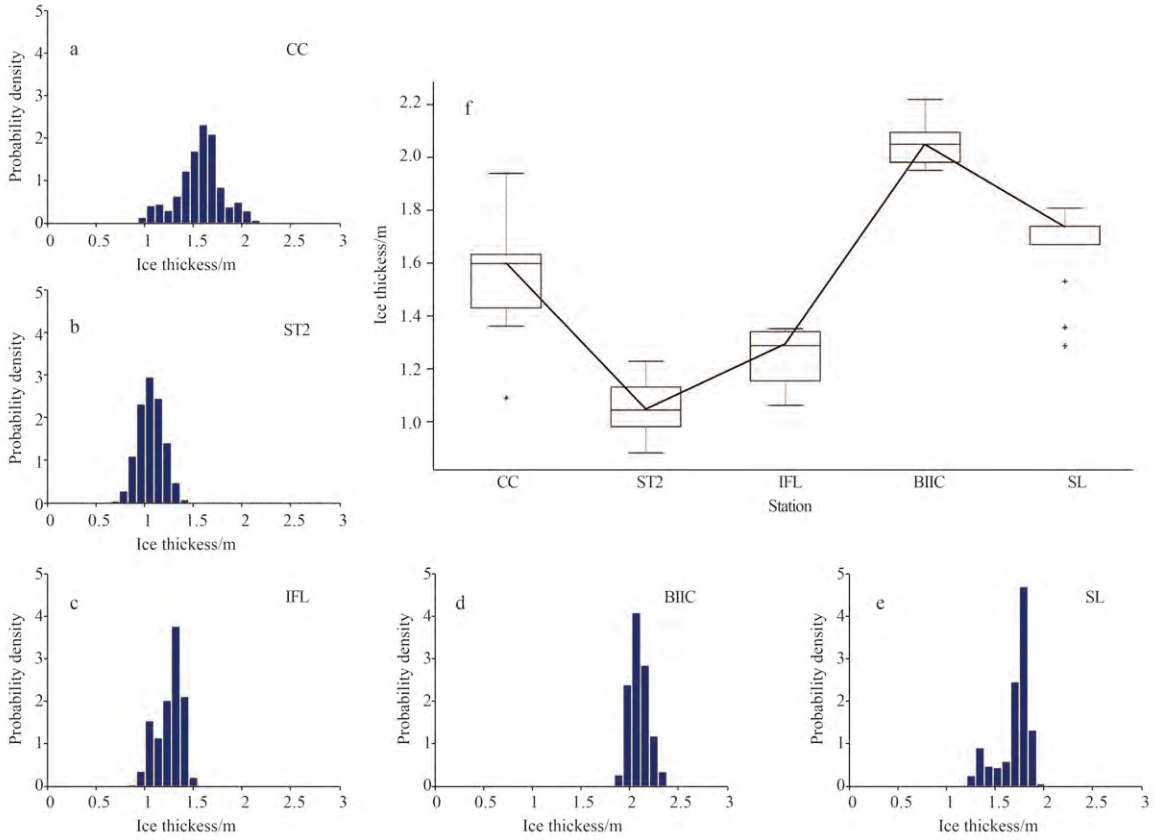

Fig. 4. Thickness statistics of the undeformed ice in the Canadian Archipelago shelf. a–e. Probability Density of ice thickness at CC, ST2, IFL, BIIC and SL, and f. statistical variables such as minimum, lower quartile, median (dashed line), upper quartile and maximum of ice thickness at each station are shown.

Table 3. Summary snow depth, ice thickness and freeboard, pulse velocity in sea ice at calibration spots and statistics of snow-covered ice thickness at stations

Station No.	Station name	Date (GMT)	Time (GMT)	North latitude	West longitude	Stage of sea ice	H_{di}/m	H_f/m	H_s/m	H_{MS}/m	H_m/m
Sta. 01	CC	2010/4/27	20:35:53	79°55.62'	119°34.06'	MY	1.69	0.17	0.05	1.54±0.22	1.60
Sta. 02	ST2	2010/4/28	22:31:47	78°59.17'	115°22.48'	FY	1.04	0.08	0.08	1.05±0.11	1.04
Sta. 03	BIIC	2010/4/30	13:42:36	78°15.84'	112°3.89'	MY	2.05	ND	0.00	2.05±0.09	2.05
Sta. 04	IFL	2020/4/30	18:20:01	78°28.93'	113°25.66'	FY	1.23	0.07	0.06	1.24±0.13	1.29
Sta. 05	SL	2010/4/30	20:31:47	77°48.95'	107°29.57'	MY	1.70	0.16	0.08	1.67±0.16	1.74

Notes: H_{di}: drill–hole ice thickness; H_f: ice freeboard; H_s: snow depth; H_{MS}: mean±standard deviation of ice thickness; H_m: median of ice thickness; MY: multiyear ice; FY: first year ice; and ND: not determined.

4 Conclusions

The GPR measurements of sea ice thickness were conducted in spring 2010 in the Canadian Arctic shelf. Five stations were selected along with a section of 350 km to study the distribution feature of sea ice thickness northern Canadian Arctic Archipelago.

Based on our experiments, an effective means to get more clear radar scans in the regional ice distribution has been confirmed, which is to make the GPR survey lines in the cross way instead of the parallel tracks to each other. The reason is the anisotropy of sea ice crystal, which will result in a weak reflection of the radar signal on the ice-water interface when the antenna field oriented perpendicular to the *c*-axis of the crystal platelets. In addition, the calculation of the sea ice thickness from GPR signals requires a penetrating velocity of the pulse in the ice that will decide the accuracy of ice thickness. So the *in-situ* calibration over known ice thickness is necessary to determine the velocity of the incident wavelet.

The mean undeformed ice thickness in both sides of the flaw lead north Borden Island were (1.05±0.11) m (ST2) and (1.24±0.13) m (IFL) respectively, which were the typical first-year ice originated from the refrozen flaw lead. At the southernmost station (SL), nevertheless, the undeformed sea ice thickness was around (1.67±0.16) m, which was significantly thinner than that

of 3–5 m at the same area in 1970s (Melling, 2002). Analogously, undeformed pack ice thickness at northernmost station (CC) was (1.54±0.22) m, comparing to the ridged ice with 2.5–3 m thick here. The maximum ice thickness sampled at Sta. BIIC southwestern coast of the Borden Island was (2.05±0.09) m, which represented the coastal fast ice in the study area.

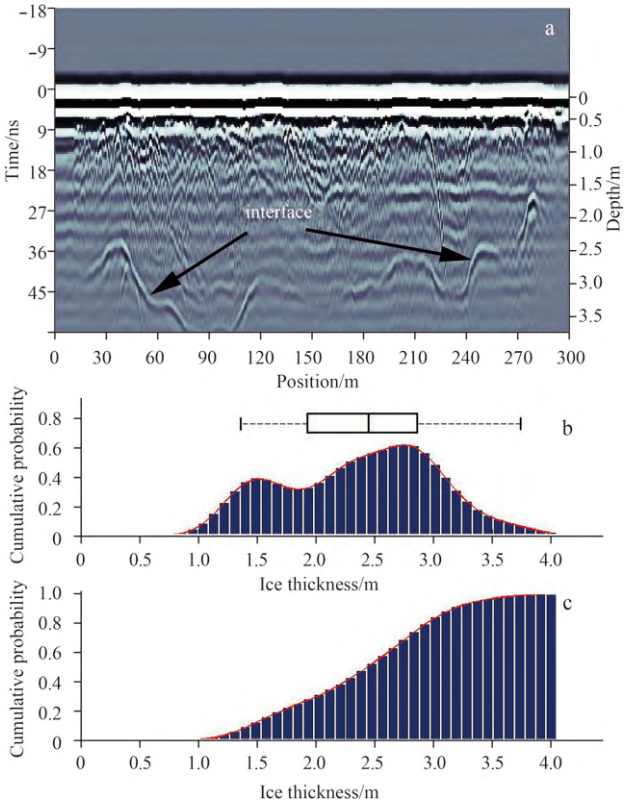

Fig. 5. GPR impulse section (a), distributions of probability density (b) and cumulative probability density (c) of ice ridge thickness at Sta. CC. The interface of sea ice and water is shown clearly on the panel a. Two extremes of probability density are occurred at thickness of 1.5 and 2.8 m with a median of 2.4 m on the panel b. The ridged ice thickness here in 80% area was less 3.0 m shown on the panel c.

It must be noticed that the snow depth of (5–10) cm at five stations has not been considered separately in the thickness calculations of sea ice. Thereby, the "sea ice thickness" here is actually presenting that of snow-plus-sea ice which is sometimes called as slab thickness (Galley et al., 2009). Due to the snow in the study area was thin and spatially homogeneous, it was reasonable to call the slab thickness as sea ice thickness. However, a little error should be kept in mind because of the various penetrating velocity in ice and snow and snow fraction within the slab column. The GPR measurements of sea ice thickness in this article are meaningful efforts to examine sea ice in the remote and severe polar region. For all that, the great amount of ice thickness dataset is still need to study the long-term and basin-scale variations in sea ice conditions and its responding mechanisms.

Acknowledgements

The author would like to thank the Polar Continental Shelf Program of Canada for the logistic supply and Ryan Galley's helps in the GPR applications.

References

Agnew T, Lambe A, Long D. 2008. Estimating sea ice area flux across the Canadian Arctic Archipelago using enhanced AMSR–E. Journal of Geophysical Research, 113(C10): C10011, doi: 10.1029/2007JC004582

Bi Haibo, Huang Haijun, Su Qiao, et al. 2014. An Arctic sea ice thickness variability revealed from satellite altimetric measurements. Acta Oceanologica Sinica, 33(11): 134–140

Bourke R H, Garrett R P. 1987. Sea ice thickness distribution in the Arctic Ocean. Cold Regions Science and Technology, 13(3): 259–280

Comiso J C. 2006. Abrupt decline in the Arctic winter sea ice cover. Geophysical Research Letters, 33(18): L18504, doi: 10.1029/2006GL027341

Comiso J C. 2012. Large decadal decline of the Arctic multiyear ice cover. Journal of Climate, 25(4): 1176–1193

Conyers L B. 2004. Ground–Penetrating Radar for Archaeology. 2nd ed. Toronto: AltaMira Press

Deser C, Teng Haiyan. 2008. Evolution of Arctic sea ice concentration trends and the role of atmospheric circulation forcing, 1979–2007. Geophysical Research Letters, 35(2): L02504, doi: 10.1029/2007GL032023

Dickins D F, Wetzel V F. 1981. Multi–ypressure ridge study, Queen Elizabeth Islands. Paper presented at the 6th international Conference POAC'81, Quebec, Canada

Galley R J, Trachtenberg M, Langlois A, et al. 2009. Observations of geophysical and dielectric properties and ground penetrating radar signatures for discrimination of snow, sea ice and freshwater ice thickness. Cold Regions Science and Technology, 57(1): 29–38

Haas C, Gerland S, Eicken H, et al. 1997. Comparison of sea-ice thickness measurements under summer and winter conditions in the Arctic using a small electromagnetic induction device. Geophysics, 62(3): 749–757

Haas C, Hendricks S, Eicken H, et al. 2010. Synoptic airborne thickness surveys reveal state of Arctic sea ice cover. Geophysical Research Letters, 37(9): L09501, doi: 10.1029/2010GL042652

Haas C, Nicolaus M, Willmes S, et al. 2008. Sea ice and snow thickness and physical properties of an ice floe in the western Weddell Sea and their changes during spring warming. Deep–Sea Research Part II: Topical Studies in Oceanography, 55(8–9): 963–974

Hansen E, Gerland S, Granskog M A, et al. 2013. Thinning of Arctic sea ice observed in Fram Strait: 1990–2011. Geophysical Research Letters, 118(10): doi: 10.1002/jgrc.20393

Harper J T, Bradford J H. 2003. Snow stratigraphy over a uniform depositional surface: spatial variability and measurement tools. Cold Regions Science and Technology, 37(3): 289–298

Holt B, Kanagaratnam P, Gogineni S P, et al. 2009. Sea ice thickness measurements by ultrawideband penetrating radar: First results. Cold Regions Science and Technology, 55(1): 33–46

Howell S E L, Duguay C R, Markus T. 2009. Sea ice conditions and melt season duration variability within the Canadian Arctic Archipelago: 1979–2008. Geophysical Research Letters, 36(10): L10502, doi: 10.1029/2009GL037681

Howell S E L, Wohlleben T, Dabboor T, et al. 2013. Recent changes in the exchange of sea ice between the Arctic Ocean and the Canadian Arctic Archipelago. Journal of Geophysical Research: Oceans, 118: 3595–3607, doi: 10.1002/jgrc.20265

Johnston M E, Masterson D, Wright B. 2009. Multi–year ice thickness: Knowns and unknowns. Paper presented at the 20th POAC Conference. Lulea, Sweden: Lulea University of Technology

Kovacs A, Morey R M. 1978. Radar anisotropy of sea ice due to preferred azimuthal orientation of the horizontal c axes of ice crystals. Journal of Geophysical Research, 83(C12): 6037–6046

Kovacs A, Morey R M. 1979. Anisotropic properties of sea ice in the 50– to 150–MHz range. Journal of Geophysical Research, 84(C9): 5749–5759

Kovacs A, Morey R M, Cox G F N. 1987. Modeling the electromagnet-

ic property trends in sea ice, part I. Cold Regions Science and Technology, 14(3): 207–235

Kwok R, Cunningham G F. 2010. Contribution of melt in the Beaufort Sea to the decline in Arctic multiyear sea ice coverage: 1993–2009. Geophysical Research Letters, 37(20): L20501, doi: 10.1029/2010GL044678

Kwok R, Cunningham G F, Wensnahan M, et al. 2009. Thinning and volume loss of the Arctic Ocean sea ice cover: 2003–2008. Journal of Geophysical Research, 114(C7): C07005, doi: 10.1029/2009JC005312

Kwok R, Rothrock D A. 2009. Decline in Arctic sea ice thickness from submarine and ICESat records: 1958–2008. Geophysical Research Letters, 36(15): L15501, doi: 10.1029/2009GL039035

Li Zhijun, Zhang Zhanhai, Lu Peng, et al. 2005. Some parameters in arctic sea ice dynamics from an expedition in the summer of 2003. Acta Oceanologica Sinita, 24(6): 54–61

Mclaren A S, Wadhams P, Weintraub R. 1984. The sea ice topography of M'Clure Strait in winter and summer of 1960 from submarine profiles. Arctic, 37(2): 110–120

Melling H. 2002. Sea ice of the northern Canadian Arctic Archipelago. Journal of Geophysical Research, 107(C11): 3181, doi: 10.1029/2001JC001102

Millero F J, Leung W H. 1976. Thermodynamics of seawater at one atmosphere. American Journal of Science, 276(9): 1035–1077

Pälli A, Kohler J C, Isaksson E, et al. 2002. Spatial and temporal variability of snow accumulation using ground-penetrating radar and ice cores on a Svalbard glacier. Journal of Glaciology, 48(162): 417–424

Pilon J A, Allard M, Seguin M K. 1992. Ground Probing Radar in the investigation of permafrost and subsurface characteristics of surficial deposits in Kangiqsualujjuaq, northern Quebec. In: Pilon J A, ed. Geological Survey of Canada. Ottawa, 165–175

Rothrock D A, Yu Y, Maykut G A. 1999. Thinning of the Arctic sea-ice cover. Geophysical Research Letters, 26(23): 3469–3472, doi: 10.1029/1999GL010863

Sinisalo A, Grinsted A, Moore J C. 2003. Snow-accumulation studies in Antarctica with ground-penetrating radar using 50, 100 and 800 MHz antenna frequencies. Annals of Glaciology, 37(1): 194–198

Stefan J. 1891. The theory of ice formation, especially regarding ice formation in the Polar Sea. Annalen der Physik und Chemie, 42: 269–286

Stroeve J C, Kattsov V, Barrett A, et al. 2012. Trends in Arctic sea ice extent from CMIP5, CMIP3 and observations. Geophysical Research Letters, 39: L16502, doi: 10.1029/2012GL052676

Trachtenberg M A. 2008. Investigating the response of ground penetrating radar over snow covered sea ice [dissertation]. Manitoba: University of Manitoba

Tivy A, Howell S E L, Alt B, et al. 2011. Trends and variability in summer sea ice cover in the Canadian arctic based on the Canadian ice service digital archive, 1960–2008 and 1968–2008. Jounal of Geophysical Research, 116(C3): C03007, doi: 10.1029/2009JC005855

Wadhams P. 2006. Arctic sea ice thickness—a review of current technology and future possibilities. In: Wadhams P, Amanatidis G, eds. Arctic Sea Ice Thickness: Past, Present and Future. Belgium: European Communities, 14–18

Wadhams P, Hughes N, Rodrigues J. 2011. Arctic sea ice thickness characteristics in winter 2004 and 2007 from submarine sonar transects. Jounal of Geophysical Research, 116(C8): C00E02, doi: 10.1029/2011JC006982

Winther J G, Bruland O, Sand K, et al. 1998. Snow accumulation distribution on Spitsbergen, Svalbard, in 1997. Polar Research, 17(2): 155–164

Winebrenner D P. 1989. Sea ice characterization measurements needed for testing of macrowave remote sensing models. IEEE journal of Oceanic Engineering, 14(2): 149–158